Tailoring plasmonic substrates for surface enhanced spectroscopies

Surbhi Lal,[ae] Nathaniel K. Grady,[ae] Janardan Kundu,[be] Carly S. Levin,[be] J. Britt Lassiter[de] and Naomi J. Halas*[abce]

Received 18th March 2008
First published as an Advance Article on the web 31st March 2008
DOI: 10.1039/b705969h

Our understanding of how the geometry of metallic nanostructures controls the properties of their surface plasmons, based on plasmon hybridization, is useful for developing high-performance substrates for surface enhanced spectroscopies. In this *tutorial review*, we outline the design of metallic nanostructures tailored specifically for providing electromagnetic enhancements for surface enhanced Raman scattering (SERS). The concepts developed for nanoshell-based substrates can be generalized to other nanoparticle geometries and scaled to other spectroscopies, such as surface enhanced infrared absorption spectroscopy (SEIRA).

Introduction

Since the initial discovery of enormous Raman signals from molecules adsorbed on roughened silver electrodes,[1,2] it is now well understood that nanoscale features on metallic surfaces are responsible for the enhancement of Raman scattering. Subsequent development of various substrates and a physical understanding of the phenomenon show that nanoscale features on a metallic surface can support strong fields that are significantly enhanced relative to the incident field illuminating the surface. This enhanced near field is responsible for the giant Raman signals observed from molecules located within the enhanced near field. This phenomenon is known as surface enhanced Raman scattering (SERS).

Understanding how the local electromagnetic environment enhances the spectral response of adsorbate molecules has garnered intense scientific interest. Single molecule SERS observations from dye molecules adsorbed on aggregated colloid substrates,[3,4] and the ensuing controversy over the magnitude of the field enhancement that makes single molecule detection possible, has also spurred great interest in SERS, specifically, in what properties of colloidal aggregates give rise to large enhancement factors. It is now well accepted that virtually all single molecule SERS signals detected in colloidal aggregates result from pairs of directly adjacent metallic nanoparticles and not from single isolated metallic nanoparticles. The region between nanoparticle pairs contains "hot spots" or regions of intense electromagnetic fields that give rise to the enormous enhancement factors required to observe single molecule SERS. Raman-active molecules trapped in these hot spots generate SERS signals when illuminated with light of a wavelength appropriate for exciting the hot spots.

[a] *Department of Electrical and Computer Engineering, Rice University, 6100 Main Street, Houston, Texas 77005, USA. E-mail: halas@rice.edu*
[b] *Department of Chemistry, Rice University, 6100 Main Street, Houston, Texas 77005, USA*
[c] *Department of Bioengineering, Rice University, 6100 Main Street, Houston, Texas 77005, USA*
[d] *Department of Physics and Astronomy, Rice University, 6100 Main Street, Houston, Texas 77005, USA*
[e] *The Laboratory for Nanophotonics, Rice University, 6100 Main Street, Houston, Texas 77005, USA*

(Left to right) J. Britt Lassiter, Nathaniel K. Grady, Carly S. Levin, Janardan Kundu, Surbhi Lal

Surbhi Lal is a post doctoral associate in the Halas Nanophotonics laboratory. Nathaniel Grady, Janardan Kundu, Carly Levin and Britt Lassiter are graduate students in the Halas Nanophotonics Laboratory.

Naomi Halas

Dr Naomi Halas is currently Professor of Electrical and Computer Engineering, Chemistry, and Bioengineering at Rice University. She is best known scientifically as the inventor of nanoshells. She is co-founder of Nanospectra Biosciences, Inc., a company currently commercializing photothermal cancer therapy based on nanoshells. She is author of more than 150 refereed publications, and has ten issued patents. She is Fellow of five professional societies: the SPIE, the IEEE, the Optical Society of America, the American Physical Society, and the American Association for the Advancement of Science.

 This journal is © The Royal Society of Chemistry 2008

Two basic phenomena give rise to hot spots. These are (1) "lightning rod" effects, and (2) hybridized plasmons. Lightning rod effects are general properties of subwavelength metal gaps or asperities not associated with plasmons. In the case of two adjacent metal structures, the incident electromagnetic field does not appreciably penetrate inside the metal, and therefore it is compressed or "squeezed" into the gap between the two structures. This general field focusing occurs for all metals in the IR and terahertz regions, where metals are essentially perfect conductors. Lightning rod effects are purely geometrical and are essentially frequency independent for wavelengths much larger than the size of the nanoparticles. In the visible and near IR region of the spectrum, field screening is much poorer. Upon illumination, subwavelength metal structures in the visible and near IR regions support collective oscillations of the conduction electrons, known as plasmons. At resonance, these collective oscillations, or plasmon resonances, give rise to intense optical fields close to their surfaces. Plasmon resonances are a function of geometry, type of metal and are frequency dependent. The electromagnetic hot spots arising from adjacent metal nanoparticle pairs result directly from the interaction of the plasmons of the two individual nanostructures to form a new "dimer" hybridized plasmon, in addition to lightning rod effects.[5]

Due to their large enhancements and compact sampling geometries, surface enhanced spectroscopies have the potential to revolutionize many technological applications of analytical chemistry, such as forensics, environmental monitoring, and biomedical diagnostics. Transitioning surface enhanced spectroscopies from the research laboratory to the realm of useful applications is currently an important challenge. Recent advances in our understanding of how metal geometries control the properties of surface plasmons are providing new methods for the precise design of substrates tailored and optimized for specific surface enhanced spectroscopies. A guiding principle for the design of plasmonic substrates is plasmon hybridization (PH). Within the plasmon hybridization framework, plasmons on adjacent nanostructures or adjacent surfaces of complex metallic geometries interact and hybridize in analogy with the wave functions of simple quantum systems described by molecular orbital theory.[6] The PH concept provides a simple and intuitive approach for determining the plasmon resonance frequencies of nanostructures of varying complexities.[7] Since interacting plasmons give rise to extremely high intensity fields that result in the largest surface enhancements, the PH concept provides direct insight for the optimization of plasmonic substrates for surface enhanced spectroscopies. The combination of plasmonic substrate design, together with expanding capabilities for fabricating metallic nanostructures, is leading to rapid advances in this field. These efforts have resulted in nanoengineered substrates with highly reproducible enhancements, precisely known near-field profiles (and therefore the effective sensing volumes), and controllable plasmon frequencies. This high level of control and reproducibility has led to the ability to tailor plasmon resonances for specific spectroscopic applications, such as surface enhanced Raman spectroscopy (SERS) and surface enhanced infrared absorption (SEIRA). Ultimately, the precise control of the electromagnetic nanoenvironment of metallic substrates will provide a foundation for researchers to cleanly separate electromagnetic excitation effects from the less-well-understood molecule-specific molecule–substrate effects, known collectively as "chemical effects."[8] In this review, we focus on the properties of plasmonic nanostructures, whose resonances can be systematically tuned *via* plasmon hybridization, as substrates for surface enhanced spectroscopies.

Plasmon hybridization (PH)

The plasmon resonances of metallic nanostructures can be described using classical electromagnetic theory. One of the earliest examples of this is Mie scattering theory, which describes the absorption and scattering of light by small particles. Mie scattering theory is an analytical solution to Maxwell's equations for an input plane wave excitation that can be easily applied to highly symmetric spheroidal nanoparticles.[9] For more complex shapes, powerful numerical methods such as the discrete dipole approximation (DDA)[10] and the finite difference time domain (FDTD)[11,12] methods can be used to predict the near and far field optical properties. Although these methods have been successfully used to model the optical properties of a variety of nanostructures, they provide little insight into the nature and origin of the plasmons.

PH is a new paradigm for understanding the origin of plasmons and intuitively predicting the plasmonic properties of metallic nanostructures.[6,13] This model provides a simple, general principle that can guide the design of metallic structures, predict their resonant energies and provides insight into the electron distribution in a nanoparticle. Although usually described by classical electromagnetic theory, plasmons exhibit certain characteristics that are directly analogous to electrons in quantum confined systems. Just as electrons in atomic orbitals interact to form molecular orbitals in molecular orbital theory, plasmons of complex nanostructures can be thought of as interacting plasmons of simpler elementary shapes that compose the complex nanostructure. For example, the plasmon resonance energies of a nanoshell (a core–shell spherical particle consisting of a dielectric core with a thin metallic shell) can be thought of as the interacting plasmons of a solid metal sphere and a spherical cavity in a metal block. Fig. 1 illustrates this analogy. The solid metal nanosphere plasmon interacts with the plasmon of the cavity in bulk gold to form the hybridized nanoshell plasmons.[6,14] The hybridized plasmons support an antisymmetric higher energy dipolar plasmon (the charge distribution on the inner and outer surface of the shell are opposite in sign) and a symmetric lower energy dipolar plasmon. The thickness of the metal shell defines the interaction distance between the sphere and cavity plasmons, leading to the well-known tunable plasmons, characteristic of nanoshells. The predicted resonant energies of a nanoshell as calculated using the PH model are in quantitative agreement with the energies calculated using Mie scattering theory.[14]

Quantitative convergence of experiment and theory

The reports of single molecule SERS (SMSERS)[3,4] and enhancement factors of 10^{15} have renewed widespread interest in SERS as an analytical technique. SMSERS observed from dye

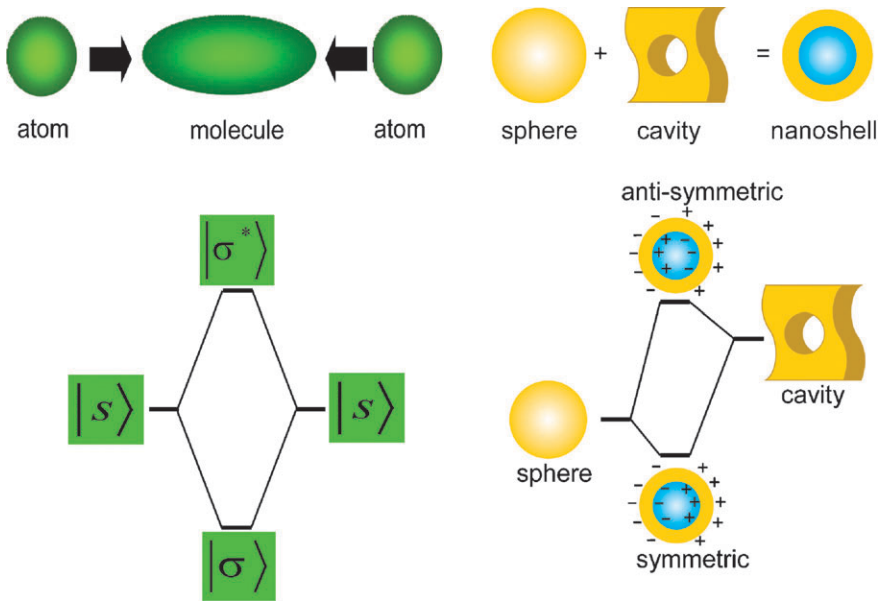

Fig. 1 Plasmon hybridization. (Left) Hybridization of interacting atomic states into molecular orbitals in a diatomic molecule. (Right) Hybridization of a nanosphere and cavity plasmon to form symmetric and anti-symmetric nanoshell plasmons.

molecules on aggregated silver colloid demonstrated that molecules with small Raman cross-sections could easily be detected due to the large SERS enhancement factors. The specificity of the SERS signal and the possibility of using near infrared excitation (compatible with probing biological samples because it eliminates autofluorescence and unwanted absorption)[15,16] have spurred renewed research in ways to reliably reproduce these SERS signals. Analysis of the aggregated colloid substrates showed that the site of the enormous enhancements consists of adjacent nanoparticles with a nanoscale interparticle gap, the hotspot geometry.[17] Although aggregated colloid substrates provide the large field enhancements needed for SERS, the lack of control and the reproducibility of the hotspots have been major limitations in the quantification of SERS.

Planar geometries such as arrays of spherical nanovoids in gold films,[18] square pyramidal pits in silicon overcoated with a thin layer of gold,[19] and gold nano bow-tie structures[20] have been designed to elicit a strong SERS response. The plasmon resonances supported by these planar structures strongly depends upon the shape and size of the nanostructures and not upon the periodicity of the structures. The facile fabrication of large area planar substrates with control over geometry and reproducible enhancement factors sufficient for SERS make these geometries highly attractive.

Several nanoparticle geometries such as triangles,[21] nanorings,[22] nanorods,[23] and nanoshells[24] support well-defined plasmon resonances. The plasmon resonances can be varied in a controlled manner by changing the dimensions of these nanoparticles. The well-defined geometry also allows for precise calculation of the plasmon resonance frequency, intensity and the spatial extent of the near field for each of these particles. Thus these well-defined geometries of nanoparticles provide a robust means of systematically designing and quantifying the SERS response to the differing plasmon resonance properties of the substrates.

Nanoshells can provide a single particle substrate with geometrically tunable plasmons that allow us to systematically investigate the SERS response as a function of plasmon frequency. Nanoshells can be tuned from the visible to the infrared regions of the spectrum in a controlled manner by varying the inner (r_1) and outer (r_2) radius of the metallic shell. The spherically symmetric geometry facilitates theoretical calculation using Mie theory of the electromagnetic near and far fields of a spherical nanoshell excited by an optical field. For the purpose of exploring SERS, this means that the spatial extent and intensity of the fields around nanoshells can be quickly and precisely evaluated for varying sizes, core–shell ratios, and dielectric environments.[25,26]

The electromagnetic SERS enhancement can be theoretically evaluated as the surface-averaged product of the electromagnetic field intensity enhancement at the incident wavelength and the enhancement at the Raman-shifted emission wavelengths: $G_{SERS} = \langle |E_{incident}(\omega_l) + E_{NS}(\omega_l)|^2 |E_{NS}(\omega_s)|^2 \rangle$, where $E_{incident}(\omega_l)$ is the field due to the incident laser at the surface of the nanostructure, E_{NS} is the enhancement of the electromagnetic field at the surface of the nanostructure, ω_l is the frequency of the excitation laser, and ω_s is the frequency of the Raman-shifted emission. Because the molecules producing the Raman signal are generally of finite extent and different parts of the molecule may experience varying fields, particularly in the case of biomolecules, G_{SERS} should either be evaluated a small distance above the surface of the nanostructure or integrated over a range of distances from the surface. The biquadratic enhancement is often further approximated as simply the quartic field enhancement at the excitation laser frequency, $|E(\omega_o)|^4$; however, it is important to keep in mind that the plasmon must have sufficient bandwidth to cover both the excitation and Raman-shifted emission frequencies. In other words, a narrow plasmon resonance would limit the enhancement of the Raman shifted photons whose frequencies do not overlap the

 This journal is © The Royal Society of Chemistry 2008

spectral bandwidth of the plasmon resonance. In the case of single molecule SERS, the surface average may be dropped and only the value of the enhancement in the vicinity of the nanostructure need be considered, for a hot spot where the individual molecule is located. There may also be an additional multiplicative factor for the "chemical enhancement" due to changes in the molecular electronic states upon adsorption to a metal surface; however, for non-resonant molecules this is a much smaller effect than the electromagnetic enhancement.[27] A discussion of the numerous theoretical techniques for the evaluation of the optical properties of plasmonic nanoparticles would easily fill several review articles. Fortunately for the interested reader, this problem has already been solved by numerous authors[28,29] (and citations therein).

Comparison of SERS enhancements in nanoshells and dimers

Historically, the design of "optimal" SERS substrates focused primarily on obtaining the largest possible near field enhancement. This approach enabled the detection of single molecules using SERS;[3,4] however, the signal reproducibility is often problematic and experiments were frequently performed by hunting around the sample for a molecule that by chance happened to reside in the perfect spot on the substrate to experience this massive enhancement. The most canonical example of such a system is the use of aggregated colloid, where one occasionally finds a perfect gap between particles providing enormous field enhancements in which a molecule resides. While obtaining reproducible methods for SMSERS remains an important goal of much research in the field, many other important applications, including those discussed later in this article, are possible with weaker but highly reproducible SERS enhancements. Over the last few years, there has been a notable shift in the development of substrates towards the needs of practical applications where high reproducibility and enhancement on open surfaces where molecules can easily adsorb are paramount.[30] Defining and comparing SERS enhancement factors in varying experimental systems is fraught with difficulty. In the following discussion, we will focus on the general concepts relevant to designing SERS substrates. The interested reader is strongly encouraged to consult the comprehensive and detailed critical discussion of the definition of SERS enhancement factors in the references cited,[31] and the associated extensive supporting information.

A recent experiment[32] in which SERS enhancements arising from several types of individual nanostructures were quantitatively compared to theoretical predictions demonstrated the importance of considering the actual signal one is trying to observe when designing SERS substrates. Specifically, the SERS signal arising from *p*-mercaptobenzoic acid (4-MBA) adsorbed onto four distinct nanostructures consisting of single nanospheres, single nanoshells, closely spaced pairs (dimers) of nanospheres, or nanoshells. *In situ* atomic force microscopy provided confirmation of each individual nanostructure's geometry. Theoretical calculations based on Mie theory and the FDTD method predicted that dimers exhibited maximum $|E|^4$ enhancements at least four orders of magnitude greater than the individual nanoparticles studied.[33] Experimentally, the nanosphere dimers produced SERS signals only one order of magnitude greater than isolated nanoshells. In light of these calculations, it was even more surprising that nanoshell dimers, which theoretically provided an order of magnitude stronger enhancement than even nanosphere dimers at the excitation wavelength employed, were experimentally found to produce signals comparable to isolated nanoshells. Carefully studying the experimental situation provides the key to understanding this discrepancy—the concentration of molecules deposited on the nanostructures was such that the surfaces were coated with the analyte molecule located randomly over the surface, whereas the theoretical predictions only considered the enhancement from the perspective of a single molecule sitting right at the position of maximum field enhancement. The situation where molecules are either coating the nanostructure or randomly located on the nanostructure corresponds to the typical situation most frequently relevant in a practical application of SERS. In such a situation, the appropriate theoretical quantity to compare to experimental observations is the surface integral of the SERS enhancement ($\int |E|^4 \mathrm{d}s$ or $\int |G_{\mathrm{SERS}}| \mathrm{d}s$), not the maximum SERS enhancement. Re-evaluating the theoretical predictions in this manner results in predictions which are indeed consistent with experimental observations. Furthermore, it is critically important to consider *where* the field enhancement is physically located on the nanostructured substrate. For example, most of the field enhancement in an aggregated nanoparticle system occurs in the gaps between particles. If the substrate is prepared before introduction of molecules, it may be difficult for many molecules to make their way into such a gap. The nanoshell dimers studied in the above measurement produced signals of similar magnitude to the isolated nanoshells, in contrast to the theoretical calculations of the integrated enhancement. The large forces between nanoshells likely resulted in bringing the nanoshell dimers into direct contact, closing the gaps and resulting in very different optical properties as compared to two directly adjacent particles with a gap, and prohibiting molecules from actually entering the gap where theoretical predictions indicate most of the enhancement would occur. In addition, many larger types of molecules of biological interest may not fit at all in such a gap. This illustrates why it is advantageous to have significant field enhancements over an open surface, as is the case for a single particle like a nanoshell. Developing such particles with large enhancements at open surfaces, for example by breaking spherical symmetry in a core–shell geometry, is currently a very active area of research.

Optimizing the dimensions of nanoshells for SERS

Armed with the theoretical tools to predict the relative efficacy of nanoparticles for a SERS substrate and the ability to create particles with precisely controlled geometries and optical properties, we can now consider the optimization of a nanostructure for a SERS experiment. A specific example is the optimization of silver nanoshells for the enhancement of Raman scattering from *p*-mercaptoaniline (*p*MA) under ambient conditions.[34,35] The optimal nanoshell structure found in this study is not specific to *p*MA; however, the optimal nanoshell geometry would change significantly if the

experiment was performed on wet samples as would be necessary for studying many biologically relevant molecules such as DNA or proteins. As is the case for most SERS experiments, a fixed excitation wavelength, specifically 782 nm, was employed for this measurement. The plasmon hybridization picture discussed above provides critical understanding of the nature of the origin of the tunable plasmon in the nanoshell geometry. For particles of dimensions comparable to the excitation wavelength, a numerical solution including the effects of phase retardation (that is the variation of the applied optical field across the nanoparticle due to the finite wavelength of light) must be employed for quantitative comparison with experimental results. Theoretically, the relative efficacy of a particular nanoshell for SERS can be evaluated by calculating the surface average G_{SERS} using Mie scattering theory for the specific Stokes-shifted Raman frequencies measured. Fig. 2(a) shows a contour plot illustrating the dependence of G_{SERS} on the experimentally controllable geometric parameters created by repeating this calculation for a range of inner (r_1) and outer (r_2) radii. For the nanoshell geometries indicated as white squares overlaying the contour plots, the average SERS enhancement is obtained experimentally by measuring the ratio of the observed Raman signal per molecule adsorbed on the nanoshell surface to the Raman signal per molecule observed in a sample of neat *p*MA. Comparison of the experimentally and theoretically obtained enhancement factors over a wide range of nanoshell geometries and Raman modes, shown in Fig. 2(b), demonstrates excellent agreement between experiment and theory. The verification by accurate electromagnetic simulations combined with the insight gained from the plasmon hybridization picture provides us with the tools needed to explore the creation of more complex substrates, such as arrays of nanoparticles[36,37] or individual nanoparticles of lower or broken symmetry.[38] In most Raman experiments or instruments, the excitation laser is fixed (*i.e.* a λ = 785 nm diode or λ = 633 nm HeNe) and the SERS substrate properties must be optimized for a particular excitation. Fundamentally it is also important to study the complementary case—given a substrate with particular plasmon resonance, how does the SERS response vary as a function of excitation wavelength? An example of such a study is one by McFarland *et al.*[39] where the SERS and far-field scattering properties of substrates with varying resonances based on nanoparticle arrays fabricated by nanosphere lithography were studied.

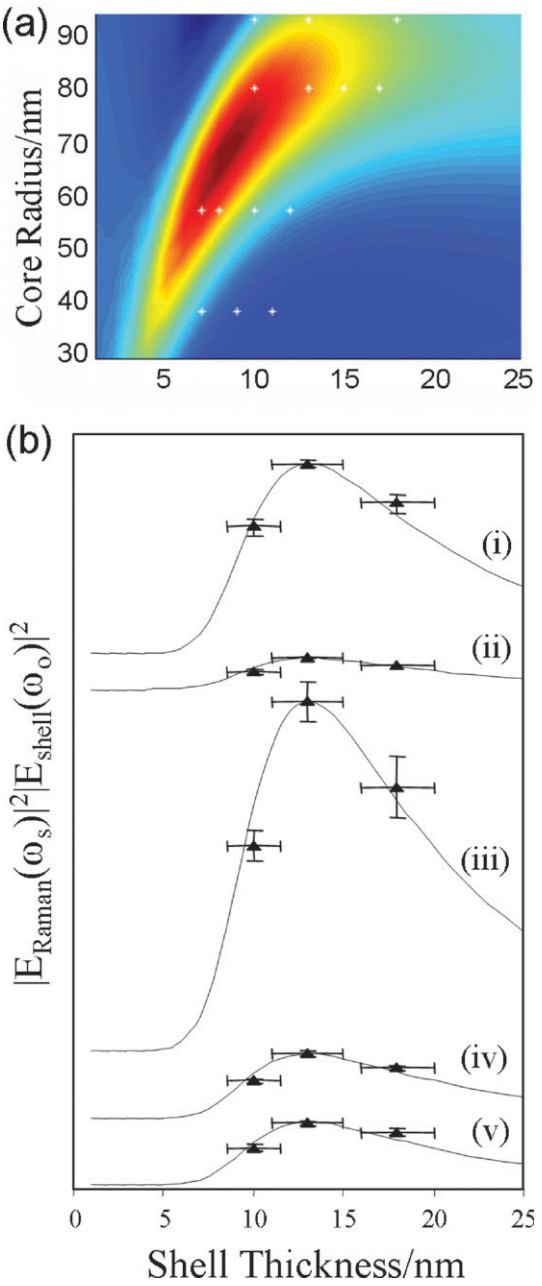

Fig. 2 (a) Calculated G_{SERS} for the 1590 cm^{-1} Raman mode as a function of core radius and silver shell thickness. The white dots indicate the fabricated nanoshell films. (b) Comparison of the measured Raman modes to theoretical calculations for 3 shells fabricated on a r_1 = 94 nm silica core. The normalized enhancement of the (i) 1590 cm^{-1}, (ii) 1180 cm^{-1}, (iii) 1077 cm^{-1}, (iv) 1003 cm^{-1}, and (v) 390 cm^{-1}. Figure reproduced from ref. 34. Copyright 2004 Proc. Natl. Acad. Sci. USA.

Profiling of the SERS enhancement above a surface: L_{SERS}

One of the most exciting areas in which surface-enhanced Raman scattering is applicable is the detection of biologically relevant molecules.[40] One large class of applications involve coating the nanostructure with an agent to capture the desired analyte, which may not naturally adsorb to the metallic surface of the plasmonic nanostructure, for example, either specifically by coating the nanostructure with a capture ligand or antibody, or nonspecifically by intercalation into an alkanethiol self-assembled monolayer (SAM)[41] or lipid bilayer[42] attached to the nanostructure. In all these applications it is critical to understand the distance profile of the SERS enhancement in the region surrounding the nanostructure to ensure the analyte molecule will actually reside in the sensing region. Calculating the distance dependence of the SERS enhancement for a given nanoparticle or film substrate is straightforward; however, demonstrating that these models accurately represent the physical nature of the experiments being carried out is far more challenging. Empirically, the

This journal is © The Royal Society of Chemistry 2008

decay profile with distance from a substrate surface can be approximated as an exponential decay with a characteristic length scale L_{SERS}, defined as the distance where the near field falls to 1/e of the field at the nanoparticle surface. For some substrates such as thin films or nanoshells, the exponential dependence is quantitative. This definition provides a useful metric for quantifying the SERS sensing volume around a given nanostructure.

To measure the distance dependence of the SERS enhancement surrounding a Au–silica nanoshell, a bifunctional molecular ruler was designed. The ruler consists of a single-stranded DNA (ss-DNA), consisting entirely of adenine bases, terminated with a fluorescein functional group on the distal end to act as a probe of the field and a thiol group on the proximal end to facilitate attachment to the nanoshell surface.[43] Varying the number of bases in the ss-DNA, illustrated in Fig. 3(a), enables precise positioning of the fluorescein terminus at controlled distances from the nanoparticle surface. Both the fluorescein moiety and the ss-DNA spacer produce distinct SERS signals that vary independently as a function of ruler length, enabling a self-consistent determination of the spatial extent of the field enhancement surrounding the nanoparticle. By measuring the *ratio* of the SERS signals from the fluorescein functional group and the adenine spacer, variations in molecular packing density and nanoparticle coverage are eliminated from the measurement. This quantity is also easily calculated using Mie theory, enabling direct verification of the functional form of the decay of the SERS effect as a function of distance from the nanoparticle surface. The SERS intensity of fluorescein is calculated at a distance above the nanoparticle surface given by the length of the adenine strand, and the intensity of the adenine signal consists of the integrated signal as a function of distance d from the nanoparticle surface, $\int_{r_2}^{r_2+d} G_{SERS} dr'$. This is directly analogous to the sum of the SERS signals from each adenine moiety at each respective chain length.

The agreement between the theoretically and experimentally derived profiles is shown in Fig. 3(b). The characteristic length scale for the SERS signal profile of the nanoshells studied in this experiment were determined to be L_{SERS} = 6.2 nm for a nanoshell with $[r_1, r_2]$ = [43, 58] nm and L_{SERS} = 9.7 nm for a nanoshell with $[r_1, r_2]$ = [70, 91] nm. This method is generally applicable to a wide range of nanoengineered plasmonic substrates, enabling the development and optimization of SERS substrates for large biomolecules and assays based on capturing analytes using a functionalized nanoparticle surface.

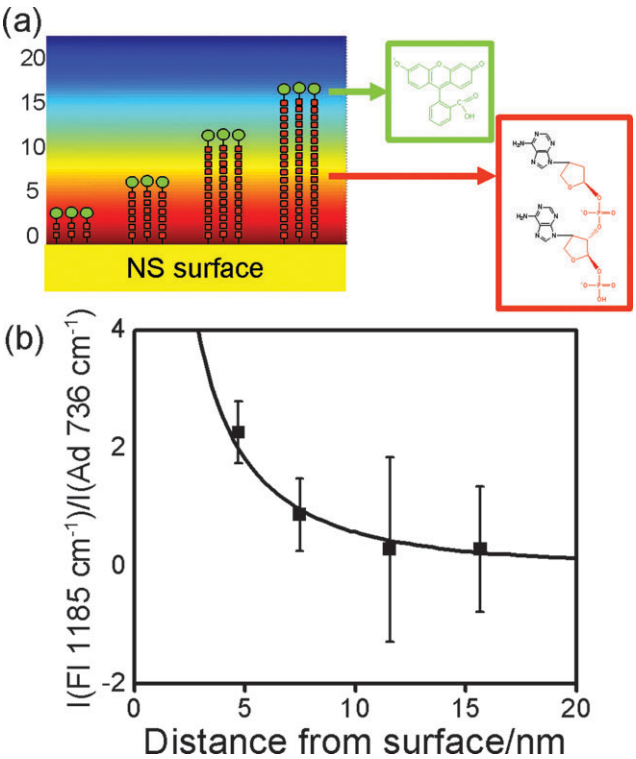

Fig. 3 (a) Schematic diagram showing the bifunctional Raman-active molecular rulers at varying distances from the nanoshell surface (*y*-axis). Both the terminal fluorescein and adenine strand moieties used as building blocks are shown. The SERS spectrum for each molecular component of the ruler provides an independent SERS spectrum dependent on the nanoparticle's near field, as described in text. (b) The ratios of SERS intensities (I(fluorescein@1185 cm^{-1})/I(adenine@736 cm^{-1})) as a function of distance from the nanoshell surface on $[r_1, r_2]$ = [43, 58] nm nanoshells. Experimental values are the black squares and the line is the theoretically calculated value. Figure reprinted with permission from ref. 43. Copyright 2006 American Chemical Society.

Implications for the design of future SERS substrates

It is clear that the conceptual understanding, theoretical tools, and experimental methods necessary to develop and optimize SERS substrates are readily available, and have been demonstrated to be effective by thorough verification against experimental results. A general paradigm that has proven effective for developing SERS substrates can be summarized as follows: first, one must consider the nature of the application. For example, it is critical to consider questions such as whether obtaining the ultimate sensitivity for detecting a single molecule is the primary goal, or whether obtaining slightly lower sensitivity but in a very reproducible manner is preferred. Is detection going to be focused on individual molecules or nanostructures, or on the average response of a plurality of molecules adsorbed onto a large number of structures? Can the analyte introduced during substrate fabrication be integrated into interstitial gaps, or does the sensing volume need to be open and accessible such that molecules can easily be accommodated into the hot spots of the substrate? Armed with this knowledge, plasmon hybridization can be employed to develop an intuitive understanding of the plasmonic properties of a particular nanostructure and guide the conceptual development of the best practical nanostructured substrate. Finally, quantitative comparison of numerical simulations and experimentally fabricated systems can be employed to efficiently optimize the geometry for the conditions of the desired application. While theoretical simulations are invaluable for identifying the relevant parameter space to investigate experimentally, it is equally important to quantitatively verify that the theoretical models actually correspond to the experimental systems fabricated.

Spectroscopic studies using designed plasmonic substrates

The complete understanding and characterization of the electromagnetic environment of the nanoshell allows us to develop nanoshell-based active structures. Here we outline an assay, a spectroscopic study, and a nanoshell based optical device to accurately determine pH in a nanoscale environment.

Quantification assay

As more nanoparticle-based diagnostic and therapeutic schemes emerge, there is a critical need to accurately quantify the molecular density and conformation of the functional moieties grafted onto the nanoparticles. A widely used polymer in many such applications is polyethylene glycol (PEG). PEG oligomers conjugated to oncological pharmaceuticals lengthen the circulation time of these molecules in the blood stream, reducing the frequency that these drugs must be administered.[44] Thiolated PEG coatings on nanorods, quantum dots, and nanoshells (used in photothermal ablation of tumors) passivate the surface and make these particles more amenable for various biomedical applications. PEG molecules adopt two different conformations when grafted onto lipid membranes: a low packing density "mushroom" conformation and a ~10 fold higher packing density "brush" confirmation.[45]

Levin *et al.* have developed a non-destructive, all optical SERS based technique to quantify the number of molecules and hence the packing density of PEG oligomers on nanoshells.[46] The method is based on creating a Langmuir isotherm from SERS peak intensity measurements of a Raman active molecule *p*-mercaptoaniline (*p*MA) adsorbed on gold nanoshells. A Langmuir isotherm relates the concentration of molecules adsorbed on a surface to the fractional coverage of the molecules on the surface. Fig. 4(a) shows a schematic of *p*MA molecules adsorbed on nanoshells used to create a Langmuir isotherm. This isotherm serves as a standard since the packing density of *p*MA on gold surfaces is well known.[47] PEG oligomers of different chain lengths conjugated to the Raman active *p*MA molecule are adsorbed on nanoshell substrates. Fig. 4(b) is a schematic of the *p*MA–PEG conjugate tagged with a fluorescent dye fluorescein attached to a nanoshell. Fig. 4(c) shows the relation between the SERS peak intensity at 1080 cm^{-1} and the fractional coverage of *p*MA on the nanoshells (assuming complete coverage when there is no further change in the SERS peak intensity with increasing concentration of *p*MA *i.e.* saturation coverage). The data follows the standard Langmuir isotherm. From this measurement the number of *p*MA molecules per nanoshell at each concentration of *p*MA can be determined, based on counting

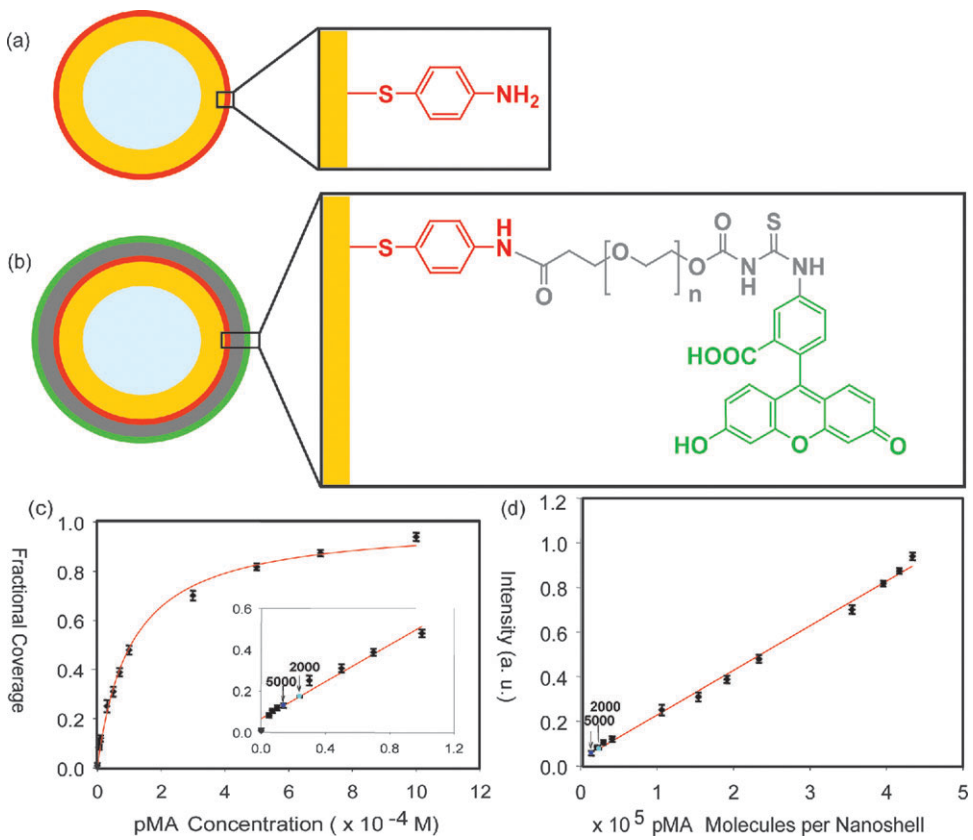

Fig. 4 (a) Self-assembly of *p*MA on a Au–silica nanoshell. (b) Self-assembly of *p*MA–PEG–fluorescein on a Au–silica nanoshell. (c) SERS intensity at 1080 cm^{-1} as a function of *p*MA concentrations (diamonds) and best-fit Langmuir isotherm (line). The inset shows the linear regime. (d) SERS intensity for various amounts of *p*MA molecules per Au–silica nanoshell. Figure reprinted with permission from ref. 46. Copyright 2006 American Chemical Society.

This journal is © The Royal Society of Chemistry 2008

the number of nanoshells in the laser spot and a 0.3 nm^2 per molecule packing density of *p*MA. Fig. 4(d) shows the concentration-dependent SERS intensity plotted as a function of *p*MA molecules per nanoshell. This plot clearly describes a linear response and is used to quantify the number of PEG molecules on the nanoshell surface. Two different sizes of PEG: 2000 MW and 5000 MW conjugated to *p*MA and fluorescein were adsorbed to nanoshells. The *p*MA SERS signal of these *p*MA–PEG–fluorescein were recorded. The concentration of the *p*MA and hence the concentration of PEG molecules was determined by interpolating the linear plot in Fig. 4(d). By this method, the packing density and conformation of PEG were determined, and found to be consistent with the denser 'brush'' confirmation of the PEG molecules on the nanoshell surface. The fluorescein tag was utilized on the PEG to provide independent quantitation of PEG in solution based on fluorescein extinction and also to provide additional assurance that the SERS signal from the PEG adsorbates was due to the presence of the entire *p*MA–PEG–fluorescein conjugate complex.

New intramolecular coupling effects in alkanethiol SAMs on nanoshells

Nanoshells provide a tunable SERS substrate. The plasmon resonance of nanoshells can be tuned to the excitation laser to optimize the integrated SERS signal enhancements. The resulting large signal enhancements allow us to probe the vibrational modes of nonresonant molecules attached to the nanoshell surface. A widely exploited family of molecules are alkanethiols that form a self-assembled monolayer (SAM) on gold and silver surfaces. Levin *et al.* have further elucidated the dependence of the gold–thiol interactions of these SAMs on the chain length of the alkanethiols.[48]

Au–silica nanoshells with core radius $r_1 = 90$ nm and $r_2 = 107$ nm were designed for optimal SERS enhancement in air at 785 nm pump laser excitation. Alkanethiols of chain lengths varying from 10–16 carbon atoms were adsorbed onto the nanoshells. Fig. 5(a) shows the unenhanced Raman spectra of the neat alkanethiols and Fig. 5(b) shows the corresponding SERS spectra. Fig. 5(a) shows the chain length dependence of the broad peak between 200–300 cm^{-1} attributed to longitudinal acoustic modes (LAM-*k*), which are analogous to the vibrations in an elastic rod. The *k* designation of the LAM modes denotes the number of internal vibrational nodes. These features are well described by simple bond polarizability models that treat the *n*-carbon molecules as a one-dimensional chain of *n* masses. The peaks in the unenhanced spectra are due to the LAM-*1* accordion mode.

In contrast to the Raman spectra, the low frequency SERS spectra in Fig. 5(b) consist of two narrow, well-defined peaks that shift to lower frequencies with increasing chain length. The SERS spectra were modeled using an extension of the bond polarizability model, treating the [Au surface]–S–$(CH_2)_n$–H as a 1D chain of $n + 1$ atoms attached to an infinitely massive surface site. The model is depicted schematically in Fig. 5(c). This simple model reproduces the observed peak intensities and shifts to lower frequencies with increasing chain length. The modified bond polarizability model also predicts that the peaks

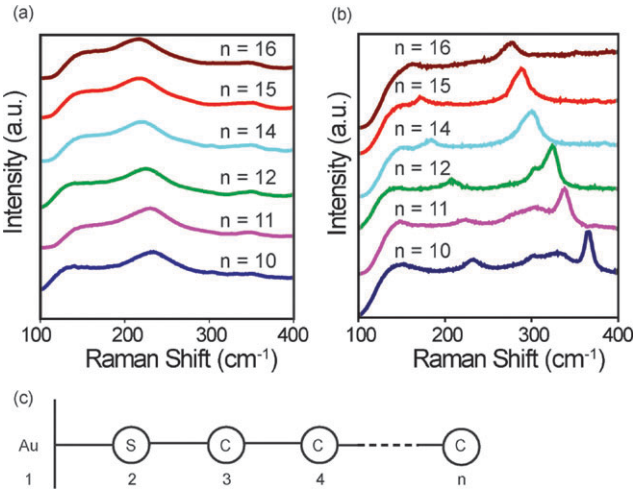

Fig. 5 (a) Unenhanced liquid Raman and (b) SERS spectra on Au nanoshells for alkanethiols HS–$(CH_2)_n$–H, where $n = 10$–16 (offset for clarity). (c) Schematic of the 1D model of the Au surface–S–$(CH_2)_n$–H self-assembled monolayer. Figure reprinted with permission from ref. 48. Copyright 2006 American Chemical Society.

arise from the coupling between the highly polarizable Au–S stretch and higher-order LAM modes of the alkane chain.

SERS based local pH "meter"

All-optical nanosensors hold exceptional promise as embeddable nanodevices that could potentially be used to probe a variety of exceedingly complex environments, such as individual living cells or the human body, in a virtually non-invasive manner.[49] The facile tunability of nanoshells allows us to design and synthesize nanoshells resonant in the near IR region. When designed to elicit a resonant optical response at near-infrared wavelengths, the spectral region of greatest physiological transmissivity, nanoshells can provide image contrast by increasing the scattered light from their immediate location without the strong absorption and fluorescence from the surrounding tissue, encountered when using visible light. Metallic nanoshells have also been shown to provide a highly localized photothermal heating response sufficient to induce cell death and to induce complete, long-term tumor remission in animal studies.[50]

Bishnoi *et al.* demonstrated an all-optical nanoscale pH meter consisting of Au nanoshells with a 4-mercaptobenzoic acid (4-MBA) adsorbate layer.[51] Fig. 6(a) is a schematic of this type of broad-range nanosensor. The nanoshells were designed for optimal use with infrared excitation and Raman emission wavelengths. The output SERS signal with pH values of the surrounding buffer ranging from 4.0 to 9.0 were recorded. As the pH of the surrounding nanoenvironment changes from acidic to basic, the carboxylic group is deprotonated. This change is prominently reflected in the changing intensity of the SERS peaks at 1702 and 1394 cm^{-1}, attributable to the C=O and COO^-, as shown in Fig. 6(b). The pH dependent SERS output is highly complex. By adapting an approach from statistical learning theory (which infers simple statistical structure from large complex data sets),[52] the dimensionality of the multispectral data set is reduced to a simple device

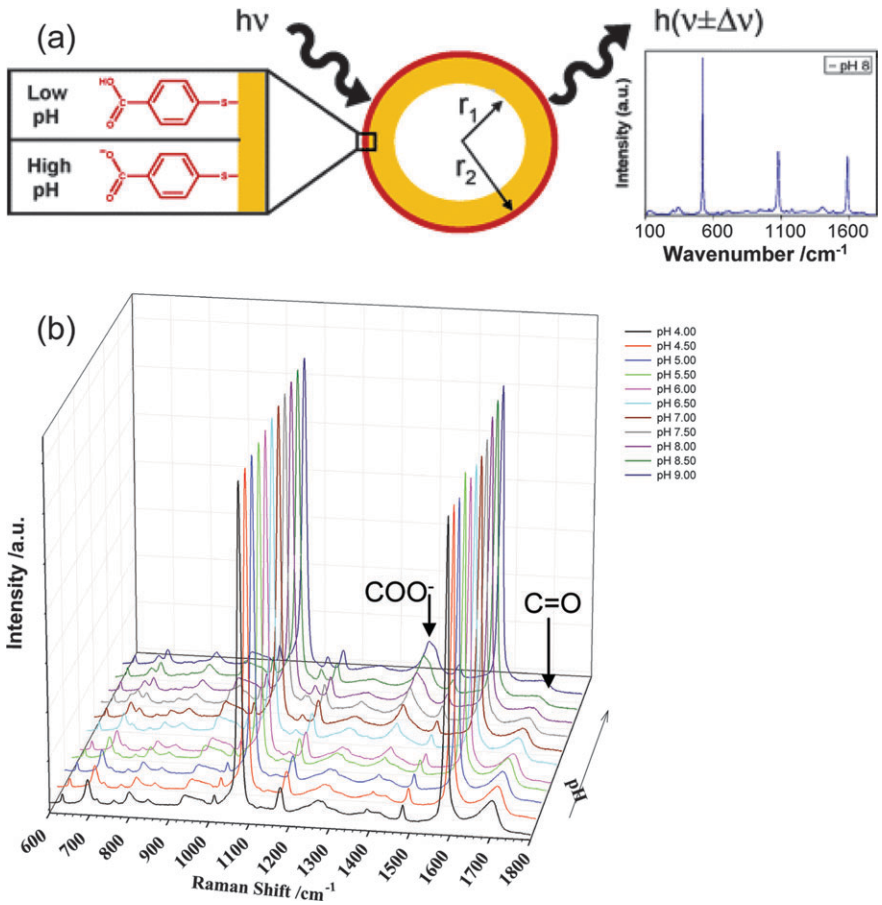

Fig. 6 (a) Schematic diagram of the Au nanoshell pH sensor, and an adsorbed monolayer of 4-mercaptobenzoic acid. The 4-MBA molecules yield a pH-dependent SERS spectrum. (b) SERS spectrum of 4-MBA on nanoshells at various pH values ranging from pH 4.0 to pH 9.0. Figure reprinted with permission from ref. 51. Copyright 2006 American Chemical Society.

characteristic. Using this characteristic curve, the pH of an unknown sample may be determined. The details of the analysis are found in ref. 51. The average accuracy of this pH nanosensor was found to be ±0.1 pH units across the physiologically relevant range of 5.8 to 7.6 pH units.

Other geometries and spectroscopies

The optical properties of symmetrical spherical nanoshells are well understood and easily predicted using PH theory. Interestingly, breaking the symmetry of the plasmonic nanostructures results in remarkable changes in the observed optical properties. The PH theory can still be applied successfully to rationalize such changes in the optical properties for a myriad of the asymmetric plasmonic nanostructures. In this section, we will summarize some of the interesting nanostructures (nanoegg and nanorice) and their optical properties as rationalized within the PH framework. The readers are urged to look into cited references for a more detailed account on the fabrication and optical properties of these nanostructures.[6,7,38,53]

Nanoeggs

Nanoeggs are reduced symmetry nanoshells in which the center of the dielectric core is offset from the center of the outer metallic shell.[7,53,54] Nanoeggs are fabricated by anisotropic deposition of additional metallic Au onto already fabricated Au nanoshells immobilized on glass substrates. The differences in the optical properties between nanoeggs and nanoshells can easily be understood using PH theory. For spherical nanoshells, the cavity and sphere plasmon mode of same angular momentum hybridize to form the nanoshell plasmon modes. On the other hand, for nanoeggs, the introduced offset core relaxes this selection rule and cavity and sphere plasmon modes of any possible angular momentum can potentially hybridize to form a greater number of optically excitable plasmon modes. As a result, even within the quasistatic limit, all of these plasmon modes of nanoeggs can be experimentally observed. Normal incidence extinction measurement on an ensemble of nanoeggs, as shown in Fig. 7(a), reveal that the spectral envelope of the plasmonic features shifts to shorter wavelengths as the offset increases, in agreement with FDTD calculations shown in Fig. 7(b). This blue shift is due to additional higher order mode mixing contributing to the extinction spectrum. These plasmon peaks of Fig. 7(a) are significantly and asymmetrically broadened due to the development of multipeaked spectra of increasing complexity, confirmed by dark field spectroscopic measurements performed on isolated, individual, randomly oriented nanoeggs with varying offset

 This journal is © The Royal Society of Chemistry 2008

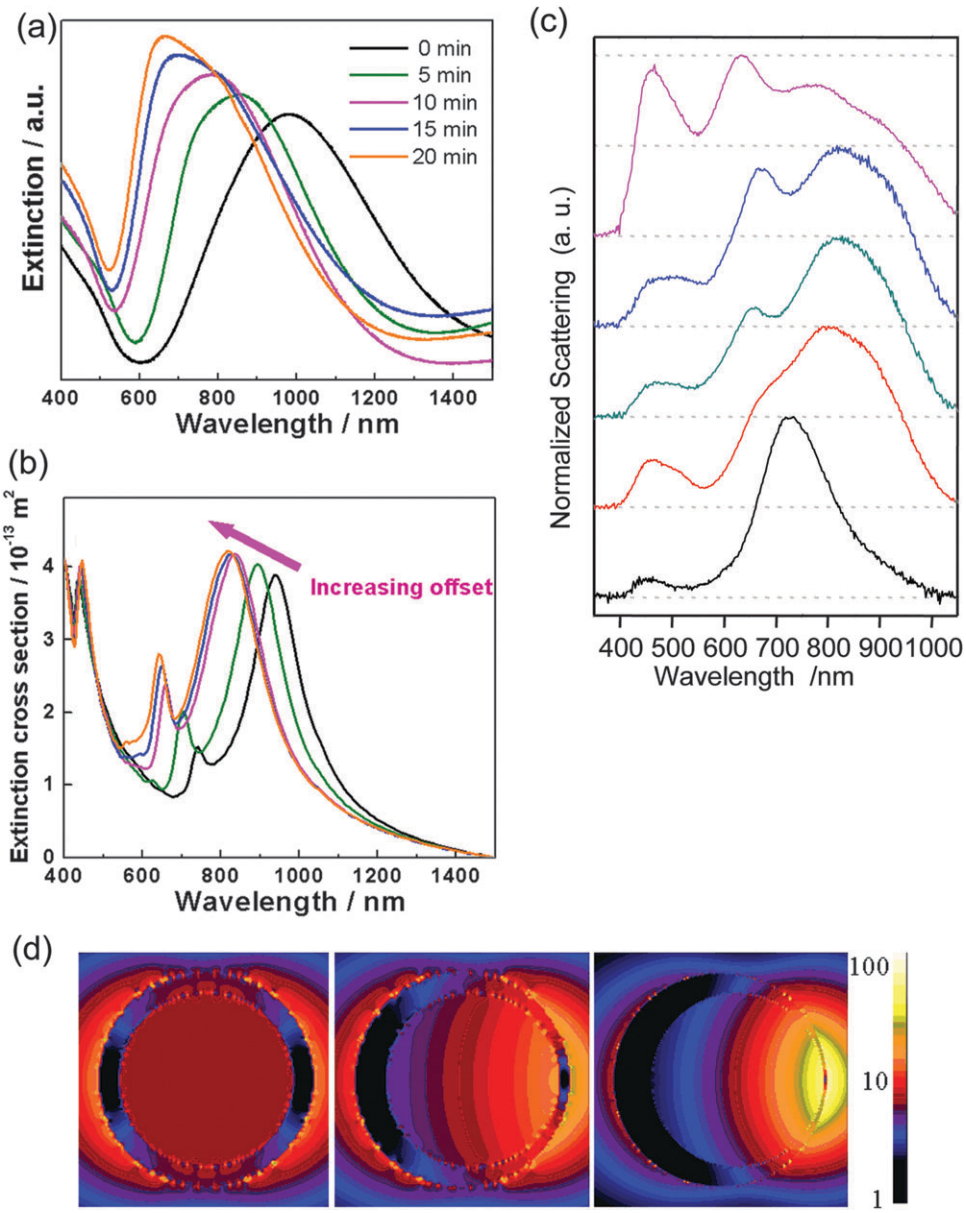

Fig. 7 (a) Experimentally measured extinction spectra of monolayers of Au nanoshell (black curve) and nanoeggs with different offsets (color curves). (Min. = minutes additional gold is deposited on the nanoshells to synthesize the nanoegg.) (b) Calculated normal incidence extinction spectra (FDTD) of reduced symmetry nanoparticles as a function of increasing offset. (c) Normalized single particle dark-field scattering spectra for a concentric nanoshell (black line) and four different non-concentric nanoshells (color lines). (d) FDTD calculated near-field plots Au nanoshells with different offset cores (silica). Left for D = 0 nm at wavelength = 641 nm. Middle is for D = 4.5 nm at wavelength = 663 nm. Right is for D = 7.5 nm at wavelength = 743 nm. Figure reproduced from ref. 53. Copyright 2006 Proc. Natl. Acad. Sci. USA.

values (Fig. 7(c)). The maximum electromagnetic field enhancements on nanoeggs are much larger than those on concentric nanoshells as shown in the FDTD calculations presented in Fig. 7(d). Although the field enhancements on nanoeggs are comparable to those attainable in nanoparticle dimer junctions,[53] in contrast to junction geometries, nanoeggs provide a region of maximum field enhancement located on the open, exterior surface of individual nanostructures and not within a narrowly confined gap or junction. This unique characteristic of nanoeggs, along with the high local field enhancements, makes them highly promising candidates for SERS substrates.

Nanorice

Nanorice are highly tunable hematite core–Au shell prolate spheroid nanoparticles that combine the plasmonic properties of nanorods and nanoshells into a single geometry.[7,38] The optical extinction spectra of nanorice, as shown in Fig. 8(a), have strong longitudinal plasmon and relatively weak transverse plasmon resonances spanning the visible to near-IR region of the electromagnetic spectrum. The longitudinal mode is seen to blueshift with increasing shell thickness. The plasmon tunability arising from changing the thickness of the shell layer is found to be far more geometrically sensitive than that arising

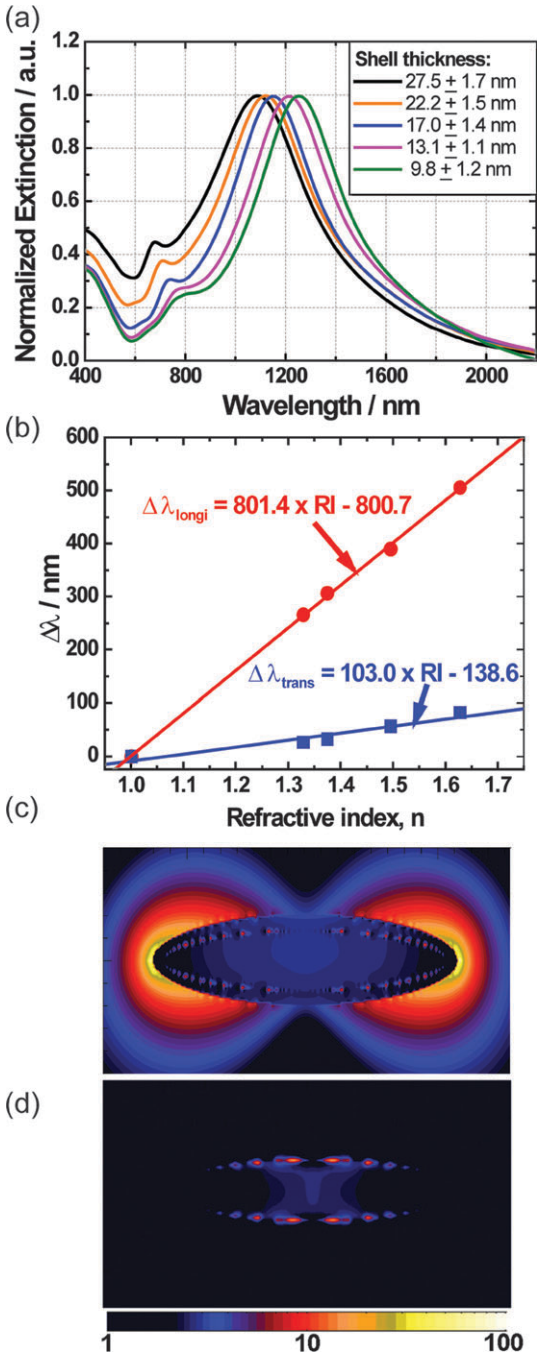

Fig. 8 (a) Extinction spectra of hematite–Au core–shell nanorice with different shell thicknesses. (b) The SPR shift of the longitudinal and transverse plasmon energies as a function of the solvent refractive index. (c) FDTD simulations for the near-field profile of the nanorice under resonance excitations: incident polarization along the longitudinal axis, λ_{exc} = 1160 nm; (d) incident polarization along the transverse axis, λ_{exc} = 860 nm. Figure reprinted with permission from ref. 38. Copyright 2006 American Chemical Society.

from varying the ellipticity of the solid parent nanostructure, a nanorod. The local fields associated with the longitudinal and transverse nanorice plasmons, calculated using FDTD, are shown in Fig. 8(c) and (d). It is observed that the asperities of this structure support very strong local field enhancements $|E|/|E_0| > 80$ at wavelengths corresponding to the longitudinal plasmon mode. These intense local fields should give rise to large SERS enhancements with the added advantage that the hot spots are completely open to the surrounding medium in this geometry. Such strong, tunable, and easily accessible local fields make this geometry highly attractive for use in designing substrates for surface-enhanced spectroscopy-based sensing. Nanorice can also be used as a localized surface plasmon resonance (LSPR) sensor since both the transverse and longitudinal plasmon resonance positions are highly sensitive to the dielectric constant of the surrounding medium. Increase in the refractive index of the surrounding solvent is accompanied by a linear redshift of the resonance positions as shown in Fig. 8(c) with a sensitivity of ~801 nm per refractive index unit for the longitudinal plasmon mode, one of the highest SPR sensitivities reported for plasmonic nanostructures. Such high environmental sensitivity of the plasmons of nanorice holds great potential for monitoring local environmental changes during various chemical and biological processes.

Nanosphere arrays for high performance and tunable SERS

The nanoscale gaps between nanoparticles in aggregate geometries support dimer plasmon hot spots, and analyte molecules trapped in these junctions experience enormous field enhancements. Plasmon hybridization theory predicts that the interparticle spacing required to achieve such large SERS enhancements is in the sub-10 nm range. Such nanoscale gaps are achievable in random nanoparticle aggregates, but are hard to reproduce controllably.

A chemical synthesis route to fabricate highly regular, ordered gold nanoparticle arrays with sub-10 nm spacing between the nanoparticles has been outlined by Wang *et al.*[37] Fig. 9(a) schematically outlines the major steps to fabricate these arrays. The fabricated nanoparticle arrays, as shown in Fig. 9(b), display a strong broad plasmon band in the near IR region as presented in Fig. 9(c). This intense broadband response is a result of the interactions between the plasmons of neighboring nanoparticles in the array. Upon illumination anywhere in this broadband, the arrays demonstrate large near field enhancements in the gaps creating a uniform density of well-defined hot spots. The arrays show an average SERS enhancement factor of $>10^8$ under near infrared (785 nm) excitation. Theoretical estimates of the local field enhancements in the junction hot spots are of the order of 10^{11} or higher.[17] The nanoparticle arrays are stable with no degradation of the SERS signal for 30 days and a loss of 50% of SERS activity after 90 days.[37] Thus nanoparticle arrays form a robust, reliable, and single substrate that can be excited using readily available multiple excitation sources in the visible to near-IR.

Combining SERS and SEIRA on the same substrate

In addition to promoting visible to near-IR excitation SERS, junction plasmons can be tuned into the mid-infrared part of the spectrum and exploited for surface enhanced infrared absorption (SEIRA) spectroscopy by direct mid-IR excitation of molecules on metal surfaces. Complementary to SERS,

This journal is © The Royal Society of Chemistry 2008

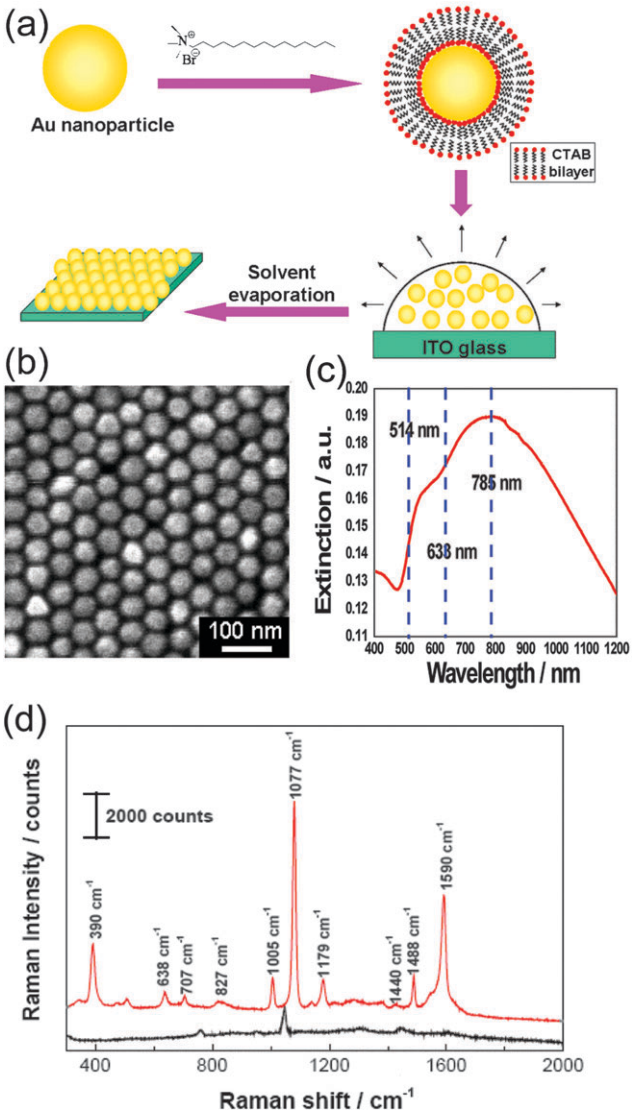

Fig. 9 (a) Schematic illustration of the fabrication of sub-10 nm gap Au NP arrays. (b) SEM image of a Au NP array on ITO glass. (c) Vis-NIR extinction spectrum of the NPs arrays (solid curve). (d) SERS spectra of *p*MA adsorbed on the Au nanosphere arrays. The red curve is a SERS spectra of *p*MA and the black curve is the spectra of Au nanoparticle arrays without *p*MA. Figure reprinted with permission from ref. 37. Copyright 2005 American Chemical Society.

SEIRA finds great practical utility in bio-chemical sensing applications for monitoring the primary dipole-active vibrational modes of organic molecules that typically absorb in the mid-IR.[55]

When nanoshells are positioned directly adjacent to each other, they also support junction or dimer plasmons in analogy with Au or Ag nanosphere aggregates or nanosphere arrays. With nanoshells whose near-field plasmon resonances are tuned to the near-IR region of the spectrum, the hot spot resonance of the nanoshell aggregate is strongly redshifted from the single particle plasmon energy, and occurs at energies in the mid-IR region of the spectrum. Both the interparticle interactions (PH) and the 'lightning rod' effect provide important mechanisms for tuning and broadening the nanoshell aggregate band far into the mid-IR, the region of interest for SEIRA. Like the Au colloidal aggregates, nanoshell aggregates are also anticipated to provide very large field enhancements within the nanoscale gaps between directly adjacent nanoshells. Recently, Kundu *et al.* have demonstrated that infrared hot spots formed in this manner provide strong enhancements of the infrared vibrational spectrum for molecule complexes with the nanoshell aggregates over a broad mid-IR spectral range.[56] FDTD simulations of the infrared hot spots characteristic of the constituent structures in the nanoshell aggregate geometry were performed for assessing the local E field strength in the junctions of nanoshells. SEIRA enhancement factors on these substrates were evaluated to be in the 10^4 range, based on a statistical evaluation of aggregate geometries combined with the FDTD modeling.[56]

The advancement of wet chemical fabrication techniques allows for the nanoshell aggregate geometry for SEIRA to be elegantly extended into nanoshell array geometry. Fabrication of highly regular nanoscale hot spots in nanoshell array is based on the assembly of near-IR resonant nanoshells into a 2D periodic array with sub-10 nm interparticle gaps.[36] The resulting nanoshell array is a unique structure that enhances SERS at near-IR wavelengths and simultaneously provides broadband mid-IR nanoscale gaps for SEIRA on the same substrate. The extinction spectrum of the nanoshell array, as shown in Fig. 10(a), consists of a narrow peak in the NIR, corresponding to the monomer nanoshell dipole, and a broad peak extending into the mid-IR region. Nanoshell arrays are demonstrated as highly efficient substrates for both SERS and SEIRA simultaneously (Fig. 10(b)). In the PH picture of a nanoshell array, the broad peak is due to the hybridization of the dipolar plasmons of the individual nanoshells that disperse strongly to lower energies in the IR region. The quadrupolar plasmons of adjacent nanoshells hybridize, forming a relatively much narrower resonance that does not disperse; its associated near-field provides the enhancements for SERS. In the near-field, the hybridization of both the dipolar and quadrupolar plasmons creates hot spots in the gaps between the nanoshells at their corresponding mid-IR and near-IR frequencies. Fig. 10(c) shows FDTD simulations of the near-field of a nanoshell array. Local field enhancements in the hot spots can be as high as 30, leading to SERS enhancement factors of 10^8–10^9, and SEIRA enhancement factors in the 10^4 range for *p*MA, a nonresonant molecule. These remarkable large enhancement factors, high reproducibility of the substrate, and well-characterized electromagnetic fields make nanoshell arrays suitable substrates for surface enhanced spectroscopy. In addition, the nanoshell arrays provide a single substrate to perform two complementary spectroscopies—SERS and SEIRA. Such rationally designed specific substrates truly unify SERS and SEIRA into the field of surface enhanced vibrational (SEV) spectroscopy and serves as a multifunctional platform for comprehensive and detailed chemical sensing.

Conclusions

Plasmon hybridization has led to a better understanding and intuition of the design parameters of nanoparticle substrates tailored to provide electromagnetic enhancements for surface

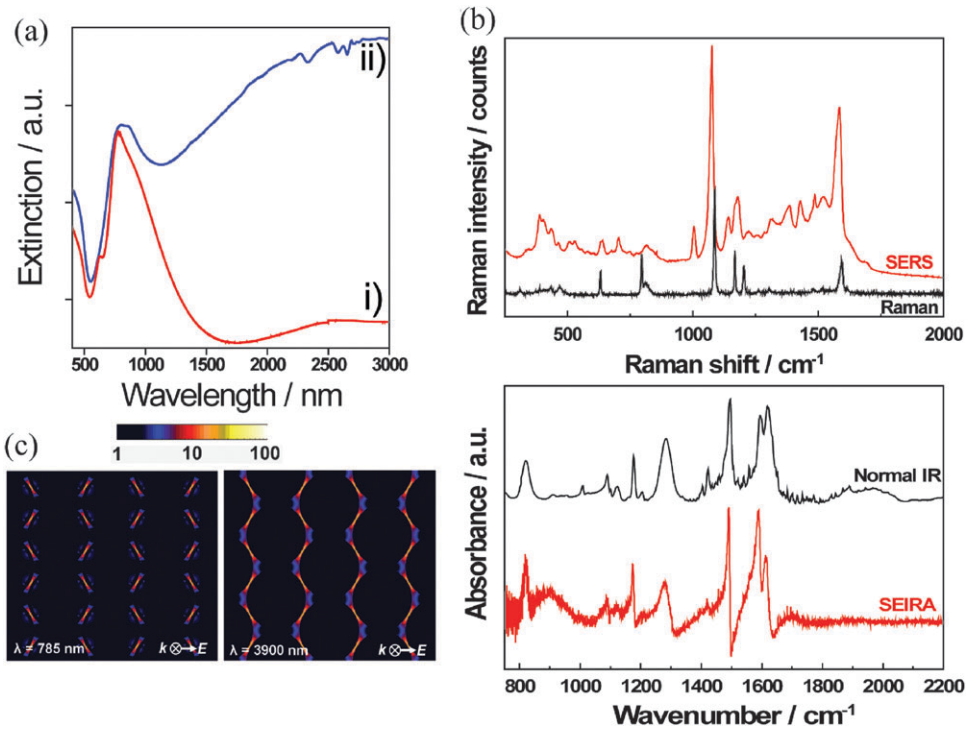

Fig. 10 Nanoshell arrays: (a) normal-incidence extinction spectra of (i) submonolayers of isolated nanoshells (red curve) and (ii) nanoshell arrays (blue curve) supported on glass slides. (b) SERS–SEIRA performance of nanoshell arrays with *p*MA as analyte molecule. For comparison purposes, both SERS and SEIRA spectra are accompanied with the corresponding normal Raman and normal IR spectra of *p*MA. Spectra are offset for clarity. (c) FDTD simulated near-field intensity ($|E|$) contours of a monolayer of hexagonally close-packed nanoshell arrays. The incident propagation and the polarization direction are shown on the figure. Figure reproduced from ref. 36. Copyright 2007 Wiley-VCH Verlag GmbH & co. Reproduced with permission.

enhanced vibrational spectroscopy. From the starting point of simple dimer and nanoshell geometries, PH theory has provided the insight for the design of symmetry breaking nanoegg particles with large EM enhancements on exposed outer surfaces, high-sensitivity nanorice particles that combine the plasmonic properties of nanoshells and nanorods, and arrays of nanospheres and nanoshells. This array geometry provides a substrate with a well-characterized electromagnetic environment and a high density of enhancing hotspots uniformly distributed over the entire substrate. The rational design of reproducible substrates with large enhancement factors provides opportunities for development of active plasmonic devices such as the pH meter, optical assays such as the determination of the packing density and conformation of PEG on nanoshells. Rationally designed substrates can be scaled to both SERS and to SEIRA, a less developed surface-enhanced spectroscopy where high performance substrates are critically needed. Combining both SERS and SEIRA enhancement capabilities on the same substrate presents revolutionary new opportunities for using surface-enhanced spectroscopies to probe molecules with multiple modalities, providing enough information-rich spectral information to, in principle, identify unknown molecular species.

Acknowledgements

We would like to acknowledge Fei Le and Peter Nordlander for the FDTD simulations of the near field of the nanoshell arrays in Fig. 10. The authors gratefully acknowledge the support of the Robert A. Welch Foundation (C-1220), the Department of Defense Multidisciplinary University Research Initiative (MURI) W911NF-04-01-0203, the NSF EEC-0304097, the NSF IGERT Fellowship of J. B. L. (DG-0504425), the NIH GCC/Keck Center Nanobiology Training Fellowship of C. S. L., and the AFOSR (F49620-03-C-0068).

References

1 M. G. Albrecht and J. A. Creighton, *J. Am. Chem. Soc.*, 1977, **99**, 5215.
2 D. L. Jeanmaire and R. P. Van Duyne, *J. Electroanal. Chem. Interfacial Electrochem.*, 1977, **84**, 1.
3 K. Kneipp, Y. Wang, H. Kneipp, L. T. Perelman, I. Itzkan, R. R. Dasari and M. S. Feld, *Phys. Rev. Lett.*, 1997, **78**, 1667–1670.
4 S. Nie and S. R. Emory, *Science*, 1997, **275**, 1102.
5 S. Maier, *Plasmonics: Fundamentals and Applications*, Springer, New York, 2007.
6 E. Prodan, C. Radloff, N. J. Halas and P. Nordlander, *Science*, 2003, **302**, 419–422.
7 H. Wang, D. W. Brandl, P. Nordlander and N. J. Halas, *Acc. Chem. Res.*, 2007, **40**, 53–62.
8 A. Otto, *J. Raman Spectrosc.*, 2005, **36**, 497–509.
9 A. L. Aden and M. Kerker, *J. Appl. Phys.*, 1951, **22**, 1242–1246.
10 B. T. Draine and P. J. Flatau, *J. Opt. Soc. Am. A*, 1994, **11**, 1491–1499.
11 M. Futamata, Y. Maruyama and M. Ishikawa, *J. Phys. Chem. B*, 2003, **107**, 7607–7617.
12 C. Oubre and P. Nordlander, *J. Phys. Chem. B*, 2004, **108**, 17740–17747.
13 E. Prodan and P. Nordlander, *J. Chem. Phys.*, 2004, **120**, 5444–5454.

 This journal is © The Royal Society of Chemistry 2008

14 E. Prodan and P. Nordlander, *Nano Lett*., 2003, **3**, 543–547.
15 K. Kneipp, H. Kneipp, I. Itzkan, R. R. Dasari and M. S. Feld, *J. Phys.: Condens. Matter*, 2002, **14**, R597–R624.
16 D. A. Stuart, J. M. Yuen, N. Shah, O. Lyandres, C. R. Yonzon, M. R. Glucksberg, J. T. Walsh and R. P. Van Duyne, *Anal. Chem*., 2006, **78**, 7211–7215.
17 H. Xu, J. Aizpurua, M. Käll and P. Apell, *Phys. Rev. E: Stat. Phys., Plasmas, Fluids, Relat. Interdiscip. Top*., 2000, **62**, 4318.
18 S. Cintra, M. E. Abdelsalam, P. N. Bartlett, J. J. Baumberg, T. A. Kelf, Y. Sugawarab and A. E. Russell, *Faraday Discuss*., 2006, **132**, 191–199.
19 N. M. B. Perney, F. J. G. d. Abajo, J. J. Baumberg, A. Tang, M. C. Netti, M. D. B. Charlton and M. E. Zoorob, *Phys. Rev. B: Condens. Matter Mater. Phys*., 2007, **76**, 035426.
20 F. Jäckel, A. A. Kinkhabwala and W. E. Moerner, *Chem. Phys. Lett*., 2007, **446**, 339–343.
21 C. L. Haynes and R. P. Van Duyne, *J. Phys. Chem. B*, 2001, **105**, 5599–5611.
22 J. Aizpurua, P. Hanarp, D. S. Sutherland, M. Käll, G. W. Bryant and F. J. Garcia de Abajo, *Phys. Rev. Lett*., 2003, **90**, 057401.
23 C. J. Murphy, T. K. Sau, A. M. Gole, C. J. Orendorff, J. Gao, L. Gou, S. E. Hunyadi and T. Li, *J. Phys. Chem. B*, 2005, **109**, 13857–13870.
24 S. J. Oldenburg, J. B. Jackson, S. L. Westcott and N. J. Halas, *Appl. Phys. Lett*., 1999, **75**, 2897–2899.
25 F. Tam, C. Moran and N. Halas, *J. Phys. Chem. B*, 2004, **108**, 17290–17294.
26 F. Tam, A. L. Chen, J. Kundu, H. Wang and N. J. Halas, *J. Chem. Phys*., 2007, **127**, 204703.
27 M. Moskovits, *Rev. Mod. Phys*., 1985, **57**, 783–828.
28 T. Wriedt, *Part. Part. Syst. Charact*., 1998, **15**, 67–74.
29 C. Girard, *Rep. Prog. Phys*., 2005, **68**, 1883–1933.
30 M. J. Natan, *Faraday Discuss*., 2006, **132**, 321–328.
31 E. C. L. Ru, E. Blackie, M. Meyer and P. G. Etchegoin, *J. Phys. Chem. C*, 2007, **111**, 13794–13803.
32 C. E. Talley, J. B. Jackson, C. Oubre, N. K. Grady, C. W. Hollars, S. M. Lane, T. R. Huser, P. Nordlander and N. J. Halas, *Nano Lett*., 2005, **5**, 1569–1574.
33 C. Oubre and P. Nordlander, *J. Phys. Chem. B*, 2005, **109**, 10042–10051.
34 J. B. Jackson and N. J. Halas, *Proc. Natl. Acad. Sci. U. S. A*., 2004, **101**, 17930–17935.
35 J. B. Jackson, S. L. Westcott, L. R. Hirsch, J. L. West and N. J. Halas, *Appl. Phys. Lett*., 2003, **82**, 257–259.
36 H. Wang, J. Kundu and N. J. Halas, *Angew. Chem., Int. Ed*., 2007, **46**, 9040–9044.
37 H. Wang, C. S. Levin and N. J. Halas, *J. Am. Chem. Soc*., 2005, **127**, 14992–14993.
38 H. Wang, D. W. Brandl, F. Le, P. Nordlander and N. J. Halas, *Nano Lett*., 2006, **6**, 827–832.
39 A. D. McFarland, M. A. Young, J. A. Dieringer and R. P. Van Duyne, *J. Phys. Chem. B*, 2005, **109**, 11279–11285.
40 H. Xu, E. J. Bjerneld, M. Käll and L. Börjesson, *Phys. Rev. Lett*., 1999, **83**, 4357–4360.
41 B. J. Kennedy, S. Spaeth, M. Dickey and K. T. Carron, *J. Phys. Chem. B*, 1999, **103**, 3640–3646.
42 C. W. Meuse, G. Niaura, M. L. Lewis and A. L. Plant, *Langmuir*, 1998, **14**, 1604–1611.
43 S. Lal, N. K. Grady, G. P. Goodrich and N. J. Halas, *Nano Lett*., 2006, **6**, 2338–2343.
44 J. M. Harris, N. E. Martin and M. Modi, *Clin. Pharmacokinet*., 2001, **40**, 539–551.
45 D. Marsh, R. Bartucci and L. Sportelli, *Biochim. Biophys. Acta*, 2003, **1615**, 33–59.
46 C. S. Levin, S. W. Bishnoi, N. K. Grady and N. J. Halas, *Anal. Chem*., 2006, **78**, 3277–3281.
47 N. Mohri, S. Matsushita and M. Inoue, *Langmuir*, 1998, **14**, 2343–2347.
48 C. S. Levin, B. G. Janesko, R. Bardhan, G. E. Scuseria, J. D. Hartgerink and N. J. Halas, *Nano Lett*., 2006, **6**, 2617–2621.
49 C. E. Talley, L. Jusinski, C. W. Hollars, S. M. Lane and T. Huser, *Anal. Chem*., 2004, **76**, 7064–7068.
50 D. P. O'Neal, L. R. Hirsch, N. J. Halas, J. D. Payne and J. L. West, *Cancer Lett*., 2004, **209**, 171–176.
51 S. W. Bishnoi, C. J. Rozell, C. S. Levin, M. K. Gheith, B. R. Johnson, D. H. Johnson and N. J. Halas, *Nano Lett*., 2006, **6**, 1687–1692.
52 C. J. C. Burges, *Geometric Methods for Feature Extraction and Dimensional Reduction*, Springer Science & Business Media, New York, 2005.
53 H. Wang, Y. Wu, B. Lassiter, C. L. Nehl, J. H. Hafner, P. Nordlander and N. J. Halas, *Proc. Natl. Acad. Sci. U. S. A*., 2006, **103**, 10856–10860.
54 Y. Wu and P. Nordlander, *J. Chem. Phys*., 2006, **125**, 124708.
55 M. Osawa, *Top. Appl. Phys*., 2001, **81**, 163–187.
56 J. Kundu, F. Le, P. Nordlander and N. J. Halas, *Chem. Phys. Lett*., 2008, **452**, 115–119.